ChemCatChem

Research Article
doi.org/10.1002/cctc.202300769

Chemistry Europe
European Chemical Societies Publishing

www.chemcatchem.org

Special Collection

Interaction and Energy Decomposition Analyses to Predict Stability of Tetraaryl Square Planar Cobalt Complexes

Manting Mu,[a] Alessandra Logallo,[b] Eva Hevia,*[b] and Max García-Melchor*[a]

The sodium-mediated cobaltation of pentafluorobenzene using the bimetallic base [NaCo(HMDS)$_3$] (HMDS=N(SiMe$_3$)$_2$) has been reported to afford a novel tetraaryl Co(II) square planar complex. Yet, the preparation of analogue structures with 1,2,3,4-tetrafluorobenzene, 1,3,5-trichlorobenzene, and 1,4-dibromo-2,5-difluorobenzene remains elusive. While the metalation step proceeds leading to stable [NaCo(HMDS)$_2$Ar] species, the ligand redistribution process to afford the tetraaryl Co(II) square planar complexes does not take place. Herein we report a density functional theory study in combination with electronic structure and energy decomposition analyses to shed light on the electronic and steric requirements to afford such complexes. Our findings show that the formation of the Co(II) square planar complexes depends on the right balance between intramolecular X···X and Na···X (X=H, F, Cl, Br) interactions. The latter further induces a *'seesaw effect'*, whereby the aryl ligand acts as a 'seesaw' allowing two X atoms in ortho positions to interdependently interact with Na. Only by considering both attractive and repulsive Na(X)···X interactions, the correct stability of the square planar complexes observed in experiments can be predicted computationally. We envision these insights to guide the rational design of novel square planar metal complexes for C–C coupling, a field that is still dominated by scarce and expensive precious metals.

Introduction

Most C–C coupling processes involve reductive elimination of organic substrates in *cis* configuration from square planar metal complexes.[1–3] While this field is riddled with examples of precious metals like Pd,[4–6] the formation of such complexes based on earth-abundant elements is still a major challenge in moving towards greener and cost-effective catalysis. On the journey to achieving this, it would be highly desirable to ease the installation of monodentate carbanion ligands (potential coupling substrates) in first-row transition metal complexes and enable the formation of these compounds in a square planar geometry. Recently, Co complexes have drawn greater attention due to its high abundance, reduced costs, and special reactivity.[3] However, the electronic configuration of the most favorable Co(II) oxidation state is d^7 instead of the desired d^8 configuration for a square planar geometry.[7] This is reflected in the literature, where only few examples of square planar Co(II) systems have been reported.[8,9] One approach to overcome the limitations in the design of such complexes is to leverage the stabilization effect through ligand chelation in combination with electronic effects. One example is the Co(II) complex reported by L. H. Doerrer *et al.*[10] featuring two bridging oxygens, as shown in Scheme 1a, and its variant with two O-bridged potassium cations, [{K(DME)$_2$}$_2$Co(DDFP)$_2$] (DME=

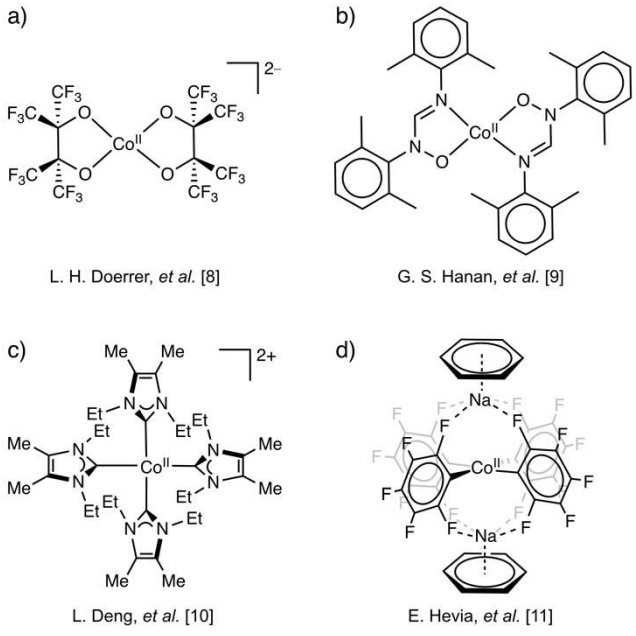

Scheme 1. Examples of reported Co(II) complexes in square planar geometry featuring bidentate and monodentate ligands.

[a] M. Mu, Prof. M. García-Melchor
School of Chemistry, CRANN and AMBER Research Centres
Trinity College Dublin
College Green
Dublin 2 (Ireland)
E-mail: garciamm@tcd.ie

[b] A. Logallo, Prof. Dr. E. Hevia
Department für Chemie, Biochemie und Pharmazie
Universität Bern
Freiestrasse 3
3012 Bern (Switzerland)
E-mail: eva.hevia@unibe.ch

Supporting information for this article is available on the WWW under https://doi.org/10.1002/cctc.202300769

This publication is part of the Catalysis Talents Special Collection. Please check the ChemCatChem homepage for more articles in the collection.

dimethoxyethane, DDFP = dodecafluoropinacolate). Neutral Co(II) species with bidentate hydroxyamidinate ligands have also been reported,[11] as well as a Co(II) species with monodentate carbene ligands which are capable of undergoing C–C bond formation processes (Scheme 1b,c).[12]

Interestingly, the complex featuring bridging oxygens in Scheme 1a portray some similarity to the tetraaryl structure $[\{Na(C_6H_6)\}_2Co(C_6F_5)_4]$ (**sq$_{FF}$**) that we recently reported (Scheme 1d),[13] featuring analogous K···O and Na···F attractive interactions. This square planar complex **sq$_{FF}$** contains four pentafluoroaryl ligands installed via Co–H exchange that bind to Co via the C that experienced metalation.

Unlike the previously reported non-ion contacted pair $\{[NBu_4]^+\}_2[Co(C_6F_5)_4]^{2-}$,[14] prepared by salt metathesis of Co(II) halide salts with LiC_6F_5, the formation of **sq$_{FF}$** does not involve the use of ultra-sensitive lithium intermediates which have many limitations.[15,16] Furthermore, previous studies have demonstrated that these tetraaryl square planar cobalt reagents can readily undergo C–C homocoupling in the presence of external oxidants such as I_2, or O_2 present in the air.[13]

Previous mechanistic investigations into the formation of $[\{Na(C_6H_6)\}_2Co(C_6F_5)_4]$ (**sq$_{FF}$**), involving the isolation of key reaction intermediates, have also revealed that initially the bimetallic base $[NaCo(HMDS)_3]$ (HMDS = bis(trimethylsilyl)amide) (**R**) promotes a Co–H exchange step to form $[NaCo(HMDS)_2(C_6F_5)]$ (**I1$_{FF}$**), which rapidly undergoes a ligand redistribution process to form **sq$_{FF}$** (Scheme 2).[13] While this two-step process also applies to other doubly *ortho*-substituted arenes (*i.e.* 1,3-difluorobenzene, 1,2,3-trifluorobenzene, 1,3,5-trifluorobenzene, 1,3,4,5-tetraflurorobenzene and 1,2,3,4-tetraflurorobenzene), when other non-doubly F-substituted arenes in *ortho* position are used, such as 1,2,3,4-tetrafluorobenzene (**Ar$_{FH}$**), 1,3,5-trichlorobenzene (**Ar$_{Cl}$**), and 1,4-dibromo-2,5-difluorobenzene (**Ar$_{Br}$**), metalation occurs to give the relevant $[NaCo(HMDS)_2(Ar)]$ intermediates. These species can be isolated and characterized,[13,17] but no ligand redistribution is observed, failing to furnish square planar complexes.

In an attempt to rationalize and predict the formation of bimetallic NaCo(II) **sq** complexes, herein we present a thorough computational study via density functional theory (DFT) calculations and various electronic structure and energy decomposition analyses, namely non-covalent interactions (NCI),[18] activation-strain (ASA)[19] and natural energy decomposition (NEDA).[20,21] Our results demonstrate the unique effect of Na···F versus Na···X (X=H, Cl, Br) interactions. The data presented in this work also shed light into intriguing deviations observed between the NCI and ASA analyses of the Na···Br interactions, which stem from the increased orbital overlap (charge transfer) in Na···X interactions involving heavier X atoms. Overall, this work provides a detailed understanding of the (in)stability of square planar Co(II) complexes, paving the way for the rational design of greener and cheaper C–C coupling catalysts.

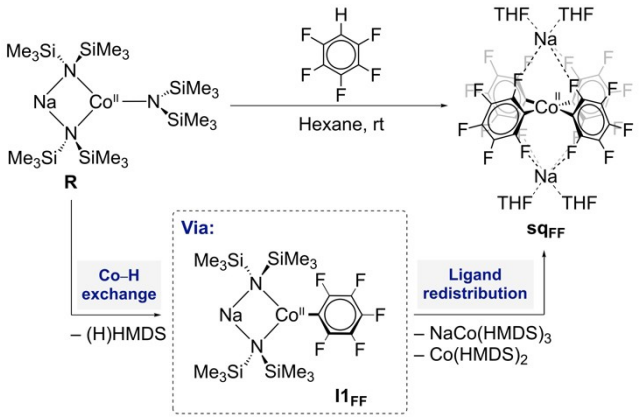

Scheme 2. Experimental findings investigating the sodium-mediated cobaltation of pentafluorobenzene using the bimetallic base $[NaCo(HMDS)_3]$.

Results and Discussion

To assess the formation of square planar NaCo(II) complexes analogous to **sq$_{FF}$** bearing different aryl substrates, we began our investigations by computing at the DFT-ωB97XD level (see Supporting Information for details) the corresponding Gibbs reaction energies at the same experimental conditions that **sq$_{FF}$** was synthesized. Further, to examine the effects of a wide range of ortho substituents in mono/doubly fluorinated compounds, lighter/heavier halogens, and hetero/homo substituents, we focused on aryls with ortho H and halogen (*i.e.* F, Cl, Br) substituents (hereafter referred to as **Ar$_{FH}$**, **Ar$_{Cl}$** and **Ar$_{Br}$**) and compared them with **Ar$_{FF}$**, which produces **sq$_{FF}$** (Scheme 1d) via C–H metalation.

Initially, we posited the formation energies of the different **sq** complexes to be correlated with the formation of the en route monoaryl intermediates **I1**. These species are formed via metalation of **Ar$_{FH}$**, **Ar$_{Cl}$**, **Ar$_{Br}$** by **R** and involve the exchange of C–H to Co–C bonds, yielding the respective monoaryl intermediates $[NaCo(\mu\text{-}HMDS)_2(C_6F_4H)]$ (**I1$_{FH}$**), $[NaCo(\mu\text{-}HMDS)_2(C_6Cl_3H_2)]$ (**I1$_{Cl}$**), and $[NaCo(\mu\text{-}HMDS)_2(C_6Br_2F_2H)]$ (**I1$_{Br}$**). These structures are analogous to each other, featuring two HMDS ligands bridging the Na and Co atoms, and the deprotonated aryl moiety bound terminally to Co, as shown in Figure 1.

As seen in Figure 1, the relative energies calculated for the different metalated aryls span a wide range of values, with **I1$_{FH}$** being the closest in energy to **Ar$_{FF}$** ($\Delta G = -4.1$ kcal/mol,

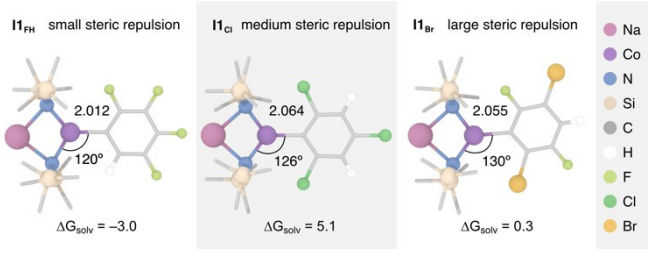

Figure 1. Optimized structures and relative Gibbs energies (in kcal/mol) calculated in benzene at 298 K and 1 atm for the formation of the monoaryl intermediates $[NaCo(\mu\text{-}HMDS)_2(Ar)]$ (**I1$_{FH}$**, **I1$_{Cl}$**, **I1$_{Br}$**) from $[NaCo(HMDS)_3]$ (**R**). Relevant bond distances (in Å) and angles are also shown.

referenced to **R**), exhibiting a +1.1 kcal/mol difference. With these data, one would expect the formation of the homoleptic tetraaryl complexes with $\mathbf{Ar_{FH}}$ and $\mathbf{Ar_{Br}}$ to be thermodynamically feasible; however, only the monoaryl product could be observed experimentally under the same reaction conditions than $\mathbf{sq_{FF}}$.[13] Hence, we can conclude that the formation energy of the monoaryl intermediates is not a good descriptor to predict the formation of the **sq** complexes; this may require the assessment of the ligand rearrangement process in monoaryl intermediates, which eventually leads to tetraaryl complexes.

The ligand rearrangement mechanism that we proposed in our recent work[13] first involves the ligand exchange between two monoaryl complexes (**I1**) to yield the bisaryl intermediate (**I2**) (Scheme 3) and the concomitant formation of the sodium cobaltate **R**. According to our DFT calculations, this process is predicted to be only slightly endergonic for the intermediates [NaCo(μ-HMDS)(μ-$C_6Cl_3H_2$)(t-$C_6Cl_3H_2$)] ($\mathbf{I2_{Cl}}$) (+5.7 kcal/mol), [NaCo(μ-HMDS)(μ-$C_6Br_2F_2H$)(t-$C_6Br_2F_2H$)] ($\mathbf{I2_{Br}}$) (+4.8 kcal/mol), but very unfavorable for [NaCo(μ-HMDS)(μ-C_6F_4H)(t-C_6F_4H)] ($\mathbf{I2_{FH}}$) (+17.6 kcal/mol). Other conformers of the bis-aryl **I2** intermediates were also considered (Figure S1) but resulted to be higher in energy compared to the species shown in Scheme 3.

Interestingly, the formation energy of the bisaryl complex $\mathbf{I2_{FH}}$ is less favorable than $\mathbf{I2_{FF}}$ (by +9.3 kcal/mol), while the analogues $\mathbf{I2_{Cl}}$ and $\mathbf{I2_{Br}}$ are much more favored, rendering the formation of these complexes to be more feasible. Nonetheless, the dimerization of the bis-metalated **I2** intermediates to afford the complexes $\mathbf{sq_{FH}}$, $\mathbf{sq_{Cl}}$, and $\mathbf{sq_{Br}}$ is predicted to be endergonic in all cases ($\geq$4.7 kcal/mol, Scheme 3). In contrast, the dimerization process for $\mathbf{sq_{FF}}$ is thermodynamically favorable by −1.90 kcal/mol, driving the overall reaction forward and releasing $Co(HMDS)_2$. This Co species can then undergo co-complexation with an extra equivalent of Na(HMDS) that can be added to the reaction mixture to form more sodium cobaltate **R**, which undergoes C–H metalation of the substrate to generate more $\mathbf{sq_{FF}}$.[13]

Intrigued by these findings, we performed further investigations which revealed that the key difference between the substrates is the substituents in *ortho* positions; this observation also explains the apparent discrepancy between the formation energies of the mono- and tetraaryl complexes, as we describe in the following. As shown in Figure 1, the most stable conformer of the monoaryl intermediates has the aryl group in terminal position. This places the ortho-substituted halide too far away to engage with the Na atom, whereas multiple Na···X interactions can be established in the **sq** complexes. To shed light on the role that these Na···X contacts play, we carried out a detailed NCI analysis on all the **sq** complexes (Figures 2a, 2b, S4 and S5).[13] The results of this analysis revealed that $\mathbf{sq_{FH}}$ lacks Na···F interactions compared to $\mathbf{sq_{FF}}$ (see Figures S5 and S4, respectively). Furthermore, there is no evidence of significant attractive interactions between Na···H, indicating that less stabilization is gained. This is in line with experimental studies which could not isolate $\mathbf{sq_{FH}}$, highlighting the importance of the Na···F contacts.[13]

Moving on to the other substrates, we observed a remarkable effect in the NCI analysis on the $\mathbf{sq_{Cl}}$ complex, shown in Figures 2a and 2c, which portrays weaker Na···Cl interactions compared to Na···F in $\mathbf{sq_{FF}}$ ($\rho = 1.33\times10^{-2}$ vs 1.52×10^{-2} a.u., respectively), displayed in Figure S4. This is somewhat unexpected since Cl is easier to polarize and has more electron density than F, and therefore one would expect a stronger interaction between Na···Cl. Upon further inspection, we could attribute the weakening of the Na···Cl contacts in $\mathbf{sq_{Cl}}$ to the '*seesaw effect*', a term that we coin in this work to describe the increase (or decrease) of an interaction caused by the interdependent contact of ortho substituted groups with the top- and bottom-Na^+ ions. Like a *seesaw*, the aryl fragment(s) $\mathbf{Ar_{Cl}}$ coordinated to Co bends towards the top or bottom Na atoms in order to establish the maximum number of Na···Cl interactions in $\mathbf{sq_{Cl}}$ (Figure 2e). Compared to $\mathbf{sq_{FF}}$, which has relatively shorter Co–C (*metalated C*) and C–F_{ortho} bond lengths (*ca.* 1.980 and 2.350 Å, respectively), $\mathbf{sq_{Cl}}$ features elongated Co–C (*metalated C*) and C–Cl_{ortho} distances (*ca.* 2.020 and 2.400 Å, respectively). The metalated $\mathbf{Ar_{Cl}}$ fragment is also relatively larger, which hinders the $\mathbf{sq_{Cl}}$ complex from establishing strong Na···Cl interactions. In addition, the *'seesaw effect'* results in one set (peak) of top- and bottom-Na···Cl interactions, as each of the $\mathbf{Ar_{Cl}}$ fragments bends either side of the Co–C bond until the interaction between both ortho-substituted Cl atoms are at their maximum contact with the Na^+ ions.

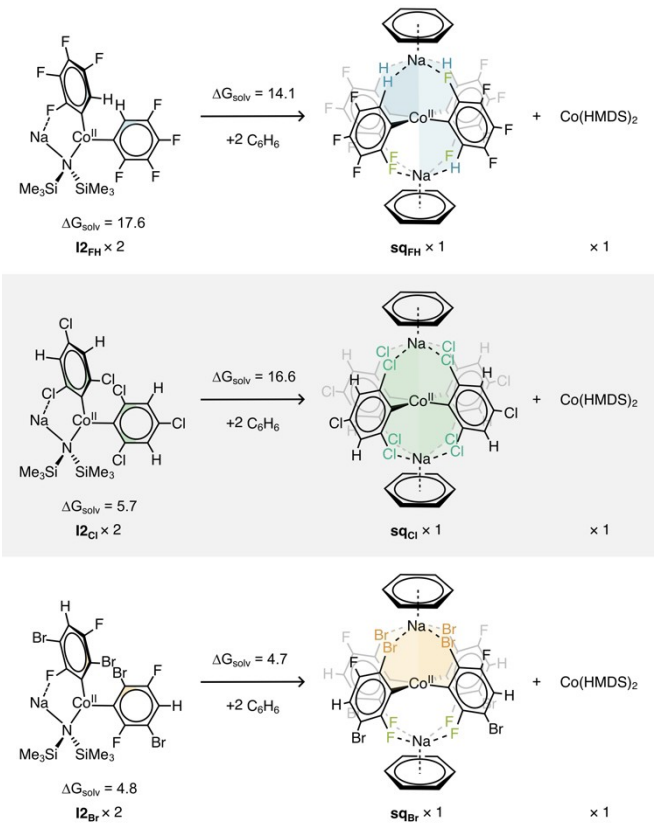

Scheme 3. Dimerization of the bisaryl intermediates [NaCo(μ-HMDS)(μ-Ar)(t-Ar)] ($\mathbf{I2_{FH}}$, $\mathbf{I2_{Cl}}$, $\mathbf{I2_{Br}}$) to form the hypothetical square planar complexes [{Na(C_6H_6)}$_2$$Na_2$Co(Ar)$_4$] ($\mathbf{sq_{FH}}$, $\mathbf{sq_{Cl}}$, $\mathbf{sq_{Br}}$). The associated Gibbs reaction energies calculated in benzene at 298 K and 1 atm are reported in kcal/mol. The relative Gibbs energies of the **I2** intermediates are referenced to **R**.

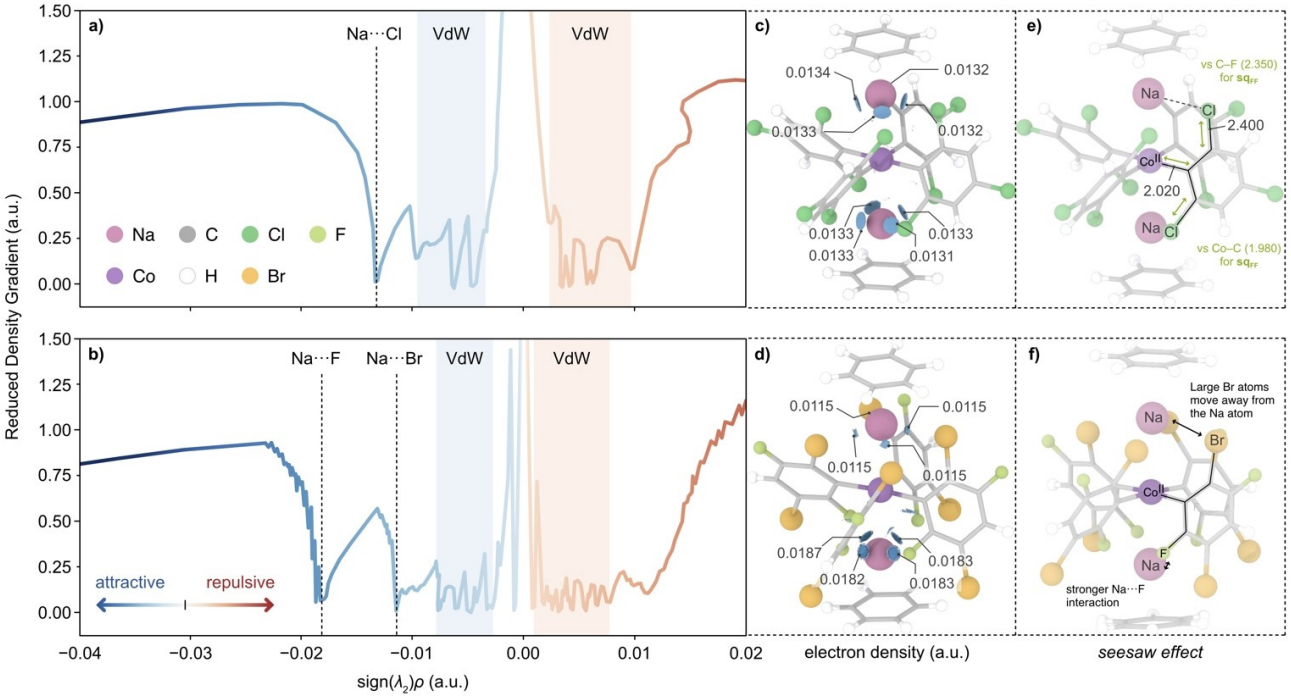

Figure 2. a) and **b)** NCI analysis on the complexes $\mathbf{sq_{Cl}}$ and $\mathbf{sq_{Br}}$, respectively, by plotting the reduced density gradient against the sign of the second eigenvalue of the Hessian matrix multiplied by the electron density (ρ), sign(λ_2)ρ. For more details about this type of analysis, see Supporting Information. In the NCI plot, attractive (repulsive) interactions are denoted by blue (red) shades; the stronger (weaker) the interaction, the darker (lighter) the shade. **c)** and **d)** representation of the most relevant NCIs as isosurfaces (isovalue = 0.6 a.u.) together with their associated ρ values (in a.u.) found in complexes $\mathbf{sq_{Cl}}$ and $\mathbf{sq_{Br}}$, respectively. **e)** and **f)** Optimized structures of $\mathbf{sq_{Cl}}$ and $\mathbf{sq_{Br}}$, respectively, to illustrate the most relevant bond lengths and the *'seesaw effect'*, respectively.

Fascinatingly, the *'seesaw effect'* plays an even more important role in the $\mathbf{sq_{Br}}$ analogue, determining the lowest energy conformation, depicted in Figure 2f. In this structure, four Br atoms interact with the same Na atom, bending the $\mathbf{Ar_{Br}}$ groups toward the Na on the opposite side to maximize the Na···Br/F contacts on both sides (Figure S2), while releasing steric hindrance. This was confirmed via NCI analysis (Figures 2b and 2d), which reveals the presence of both Na···F and Na···Br interactions with electron densities of 1.85×10^{-2} a.u. and 1.15×10^{-2} a.u., respectively. Interestingly, the Na···F interactions are predicted to be stronger than in $\mathbf{sq_{FF}}$, a direct consequence of the *seesaw effect* which pushes the Br atoms away from Na due to their larger size compared to F (r_{vdW}(Br) = 1.78 Å; r_{vdW}(F) = 1.47 Å),[22] resulting in longer and weaker Na(top)···Br contacts (Figure 2f).

While NCI plots are very insightful and indicate that Na(top)···Br contacts are weaker than Na(bottom)···F, we cannot conclude whether these Na···X interactions overall are more favorable in $\mathbf{sq_{FF}}$ than in $\mathbf{sq_{Br}}$. This is because, despite the use of the electron density within the NCI approach allows us to characterize the nature of a bond or interaction, it does not provide an accurate description of the relative strengths between different atoms (*e.g.* Na···F vs Na···Br interactions).

Hence, to quantify the strength of the different Na···X interactions in the **sq** complexes investigated herein, we performed an ASA analysis, which consists in decomposing the energy into interaction (ΔE_{int}) and distortion (ΔE_{dis}) energy terms between different fragments of a system. The ΔE_{int} term accounts for the energy gained from interactions between the fragments, while ΔE_{dis} represents the energy cost for distorting the geometry of a fragment from its isolated relaxed structure. In our analysis, the **sq** complexes were sliced into 3 separate fragments, namely top-$\{Na(C_6H_6)\}^+$, $\{Co(Ar)_4\}^{2-}$ and bottom-$\{Na(C_6H_6)\}^+$ (Figure S3). The results of this analysis are summarized in Table 1.

Firstly, we note that the total interaction energy between the three fragments in the different **sq** complexes follow a similar trend to that predicted by the NCI analysis; that is, $\mathbf{sq_{FF}}$ exhibits the largest interaction energy (*i.e.* −274.0 kcal/mol), followed by $\mathbf{sq_{Cl}}$ and $\mathbf{sq_{FH}}$. For the latter, the lower ΔE_{int} compared to $\mathbf{sq_{FF}}$ (by +9.6 kcal/mol) is mainly due to the lack of Na···F interactions. The exception in that trend is $\mathbf{sq_{Br}}$, which displays a ΔE_{int} value of *ca.* 42.0 kcal/mol lower than $\mathbf{sq_{FF}}$. To better understand this difference, instead of the total interaction energy between fragments, we computed the relative atom-specific interactions by dividing the interaction energy between the top and bottom $\{Na(C_6H_6)\}^+$ fragments and $\{Co(Ar)_4\}^{2-}$ (ΔE_{int1} and ΔE_{int2}, respectively) by the total number of Na···X contacts present between these fragments (see Table 1 and Figure S3). These specific $\Delta E_{int1,2/Na\cdots X}$ values follow the trend Na···F (0.0) > Na···Cl (+0.8) > Na···H (+2.8 and +1.2), which is identical to the results obtained in the NCI analysis, with the exception of the Na···Br interactions (−3.6), which are predicted to be stronger than the Na···F contacts in $\mathbf{sq_{FF}}$. In addition, the Na···F contacts in $\mathbf{sq_{Br}}$ also exhibit a more negative $\Delta E_{int2/Na\cdots F}$

Table 1. Summary of the computed interaction (ΔE_{int}) and distortion (ΔE_{dist}) energies, and the ratio of charge transfer relative to the polarization energy contribution ($\Delta E_{CT}:\Delta E_{POL}$) calculated via ASA and NEDA analyses, respectively (see Supporting Information for details). All the energies are given in kcal/mol. The number and type of contacts with the top and bottom $\{Na(C_6H_6)\}^+$ fragments, $Na_{top}\cdots(X)$ and $Na_{bot}\cdots(X)$, in each **sq** complex is also provided.

Complex	ΔE_{int} [a]	ΔE_{int1} [b]	$Na_{top}\cdots(X)$	$\Delta E_{int1/Na\cdots X}$ [c]	ΔE_{int2} [b]	$Na_{bot}\cdots(X)$	$\Delta E_{int2/Na\cdots X}$ [c]	ΔE_{dis1} [d]	ΔE_{dis2} [e]	$\Delta E_{CT}:\Delta E_{POL}$	$\Delta E_{CT}:\Delta E_{POL}Na\cdots X$ [f]
sq_{FF}	−274.0	0.0	4F	0.0	0.0	4F	0.0	+3.9	+0.6	13:87	13:87
sq_{FH}	−264.4	+8.5	1F+3H	+2.8	+1.2	3F+1H	+1.2	+6.9	+0.5	11:89	9:91
sq_{Cl}	−267.3	+3.4	4Cl	+0.8	+3.4	4Cl	+0.8	+3.9	+0.7	26:74	26:74
sq_{Br}	−316.1	−14.5	4Br	−3.6	−27.5	4F	−6.8	+4.5	+0.5	20:80	27:73

[a] Total interaction energy between the three fragments considered. [b] Interaction energies between the top (ΔE_{int1}) and bottom (ΔE_{int2}) $\{Na(C_6H_6)\}^+$ fragments and $\{Co(Ar)_4\}^{2-}$, referenced to sq_{FF}. [c] ΔE_{int1} and ΔE_{int2} values divided by the number of Na···X contacts, referenced to sq_{FF}. [d] Distortion energy for the $\{Co(Ar)_4\}^{2-}$ fragments. [e] Distortion energy for the top and bottom $\{Na(C_6H_6)\}^+$ fragments. These values are the same within each complex, except for sq_{FH} that are +0.5 and +0.4 kcal/mol, respectively. [f] $\Delta E_{CT}:\Delta E_{POL}$ values assuming that the charge transfer from the Na···F contacts in the hetero-substituted **sq** complexes is the same than in the homo-substituted sq_{FF} complex (see Supporting Information for details).

value than in sq_{FF} (by 6.8 kcal/mol), in agreement with the NCI analysis.

To explain the apparent discrepancy between the NCI and ASA results for the Na···Br contacts, and to gain a better understanding of the different Na···X interactions, we resorted to the NEDA analysis developed by Glendening and Streitwieser (see Supporting Information for details).[18] More specifically, herein we focus on the ratio between the charge transfer and polarization energy contributions ($\Delta E_{CT}:\Delta E_{POL}$) to the interaction energy in each of the investigated **sq** complexes. The results of this analysis, shown in Table 1, reveal an increase in the ΔE_{CT} term as we move down the halogen group (Group 17), *i.e.* Na···F (13:87) > Na···Cl (26:74) > Na···Br (27:73). These values are calculated assuming the charge transfer contribution of the Na···F contacts in the **sq** complexes to be the same as in sq_{FF} (see Supporting Information for details). This trend is in line with the more diffused nature of the *p* orbitals in larger halides. However, we note that the above trend provides a lower bound of the ΔE_{CT}(Na···Br) contribution since the Na···F interactions become stronger in sq_{Br} due to the *seesaw effect*, increasing (decreasing) the ΔE_{CT} (ΔE_{POL}) contributions. Overall, the NEDA analysis demonstrates the importance of orbital overlap in the accurate description of the Na···Br interactions, while shedding light into the disagreement between this analysis and NCI in predicting the relative strength of Na···Br and Na···F contacts in sq_{Br} and sq_{FF}, respectively. The fact that NCI predicts Na···F interactions to be stronger than Na···Br is because, despite the use of the electron density within the QTAIM approach allows to characterize the nature of a bond or interaction, it does not provide an accurate description of relative strengths between different atoms (*e.g.* Na···F vs Na···Br interactions). This is addressed in ASA, which shows that Na···Br interactions are stronger than Na···F by −3.6 kcal/mol (see Table 1).

From the ASA analysis we can also observe that the ΔE_{dis} values for the $\{Na(C_6H_6)\}^+$ fragments in the different **sq** complexes are negligible (ranging from +0.4 to +0.7 kcal/mol), whereas this term is considerably larger (*ca.* +3–6 kcal/mol) for the $\{Co(Ar)_4\}^{2-}$ units. This difference can be rationalized with the $\{Co(Ar)_4\}^{2-}$ moiety requiring a severe distortion of the square planar geometry to maximize the number of Na···X contacts. The energy penalty associated to this distortion is predicted to be even higher in sq_{FH} presumably due to the ortho H atoms from the metalated aryls which are partially positively charged, leading to repulsive interactions between these fragments and the Na^+ ions of the $\{Na(C_6H_6)\}^+$ units. We note, however, that ASA does not capture interactions within a given fragment, which is particularly important in the case of $\{Co(Ar_{Br})_4\}^{2-}$. This is evidenced by the shorter Br···Br distances in sq_{Br} compared to the bisaryl intermediate $I2_{Br}$ (3.981 vs 4.947 Å), which reflects in the endergonic formation of the sq_{Br} complex from $I2_{Br}$ (Scheme 3).

To quantify the repulsive intramolecular X···X interactions within the $\{Co(Ar)_4\}^{2-}$ fragments in the **sq** complexes, we computed their relative energies referenced to $\{Co(Ar_{FF})_4\}^{2-}$, as shown in Scheme 4. This was done by taking each of the $\{Co(Ar)_4\}^{2-}$ fragments in their respective geometries in the

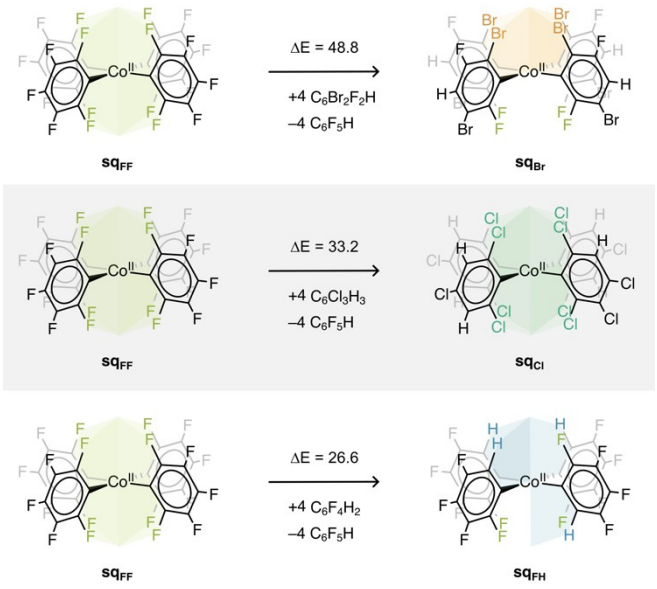

Scheme 4. Comparison of the relative stability of the different $\{Co(Ar)_4\}^{2-}$ fragments in the geometries adopted in their respective optimized **sq** complexes.

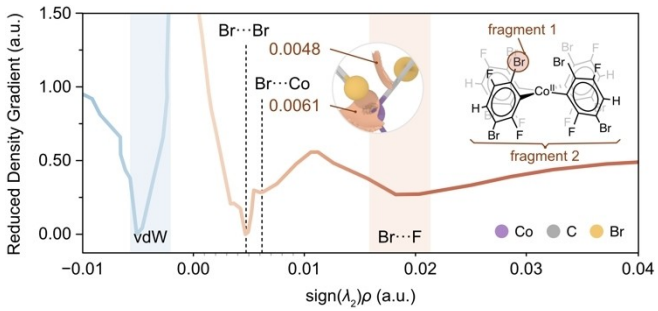

Figure 3. NCI analysis on the $\{Co(Ar_{Br})_4\}^{2-}$ unit by plotting the reduced density gradient against the sign(λ_2)ρ using $[Co(Ar_{Br})_3(C_6F_2Br)]^+$ and Br^- as fragments. Attractive (repulsive) interactions are denoted by blue (red) shades; the stronger (weaker) the interaction, the darker (lighter) the shade. The most relevant NCIs are displayed as isosurfaces (isovalue = 0.6 a.u.) in the inset, with their associated ρ values (in a.u) read out from the NCI plot.

optimized **sq** complexes and computing their energies via single-point calculations. As expected, the relative energies (in kcal/mol) correlate well with the size of X, leading to more positive values according to: $\{Co(Ar_{Br})_4\}^{2-}$ (+48.8) >> $\{Co(Ar_{Cl})_4\}^{2-}$ (+33.2) > $\{Co(Ar_{FH})_4\}^{2-}$ (+26.6). Notably, this trend differs from the monoaryl formation energies depicted in Figure 1, highlighting the importance of the substituent sterics in the formation of **sq**.

Further investigations via NCI analysis identified 4 Br···Br and 4 Br···Co contacts as the main responsible for the repulsive interactions in $\{Co(Ar_{Br})_4\}^{2-}$, with peaks centered at sign(λ_2)ρ values of 4.8×10^{-3} and 6.1×10^{-3} a.u (Figure 3). These electronic repulsions and the steric hindrance balance out the stabilization gained from the *seesaw effect*, resulting in an overall unfavorable formation of $\mathbf{sq_{Br}}$. Our calculations also show that steric effects correlate with the size of the ortho substituents (*i.e.* H < F < Cl < Br), which is also reflected in the C–Co–N bond angles observed in the monoarylated intermediates: $\mathbf{I1_{FH}}$ (120°) < $\mathbf{I1_{Cl}}$ (126°) < $\mathbf{I1_{Br}}$ (130°). Altogether, this knowledge is essential to predict the feasibility and stability of the different **sq** complexes, as we briefly describe in the following.

In the case of $\mathbf{sq_{Br}}$, the formation of this complex is not favored mainly due to the intramolecular repulsions between the Br atoms. While these interactions are reduced in the analogue complex $\mathbf{sq_{Cl}}$, the weaker Na···Cl contacts due to the *'seesaw effect'* disfavors the formation of this compound. Similarly, X···X repulsions are reduced in $\mathbf{sq_{FH}}$, but the established Na···X contacts are not sufficient to drive the formation of this complex. Only when the repulsive interactions are minimized and the strong Na···F contacts are maximized in $\mathbf{sq_{FF}}$, the formation of the square planar complex is predicted to be thermodynamically feasible, in agreement with previous experimental studies.[13]

Conclusions

In this work we report a computational study by combining DFT methods and electronic structure and energy decomposition analyses to shed light on the important role that Na···X interactions play in the stabilization of bimetallic NaCo(II) square planar complexes with general formula $[\{Na(C_6H_6)\}_2Na_2Co(Ar)_4]$. We show that the faith of these complexes depends on the right balance between attractive intramolecular Na···X and repulsive X···X (X=H, F, Cl, Br) interactions within the structure. In particular, the interplay between the bottom and top Na···X contacts results in the weakening/strengthening of these interactions which we dub as the *seesaw effect*. This explains the relative strengths of the Na···X contacts in the square planar complexes: H ($\mathbf{sq_{FH}}$) < Cl ($\mathbf{sq_{Cl}}$) < F ($\mathbf{sq_{FF}}$) < Br ($\mathbf{sq_{Br}}$). However, the formation of these complexes also depends on the intramolecular X···X repulsions, which increase with the size of the substituent X. Only when both interactions are considered, calculations predict the exclusive formation of the complex with doubly F ortho-substituted aryls ($\mathbf{sq_{FF}}$) observed in experiments. We hope these results will contribute to the design of stable Co complexes in a square planar geometry for advancing the development of more sustainable C–C coupling processes.

Acknowledgements

We thank the Irish Research Council (GOIPG/2021/88) for the financial support and the DJEI/DES/SFI/HEA Irish Centre for High-End Computing (ICHEC) for the generous provision of computational resources. EH and AL also thank the SNSF (188573) for sponsoring the experimental studies that inspired this research. Open Access funding provided by IReL.

Conflict of Interests

The authors declare no conflict of interest.

Data Availability Statement

The data that support the findings of this study are openly available in the ioChem-BD repository at https://doi.org/10.19061/iochem-bd-6-234.

Keywords: DFT calculations · bimetallic complexes · non-covalent interactions · ligand effects · electrostatic interactions · C–H metalation · cobaltation

[1] M. Pérez-Rodríguez, A. A. C. Braga, M. García-Melchor, M. H. Pérez-Temprano, J. A. Casares, G. Ujaque, A. R. de Lera, R. Álvarez, F. Maseras, P. Espinet, *J. Am. Chem. Soc.* **2009**, *131*, 3650–3657.
[2] C. P. Johnston, R. T. Smith, S. Allmendinger, D. W. C. MacMillan, *Nature* **2016**, *536*, 322–325.
[3] J. Choi, G. C. Fu, *Science* **2017**, *356*, eaaf7230.
[4] B. Fuentes, M. García-Melchor, A. Lledós, F. Maseras, J. A. Casares, G. Ujaque, P. Espinet, *Eur. J. Chem.* **2010**, *16*, 8596–8599.
[5] M. García-Melchor, M. C. Pacheco, C. Nájera, A. Lledós, G. Ujaque, *ACS Catal.* **2012**, *2*, 135–144.
[6] P. C. Andrikopoulos, D. R. Armstrong, H. R. L. Barley, W. Clegg, S. H. Dale, E. Hevia, G. W. Honeyman, A. R. Kennedy, R. E. Mulvey, *J. Am. Chem. Soc.* **2005**, *127*, 6184–6185.

[7] D. G. Barceloux, *J. Toxicol. Clin. Toxicol.* **1999**, *37*, 201–206.
[8] L. S. Merz, C. K. Blasius, H. Wadepohl, L. H. Gade, *Inorg. Chem.* **2019**, *58*, 6102–6113.
[9] Y. Gao, W.-T. Lee, V. Carta, C.-H. Chen, J. Telser, J. M. Smith, *EurJIC.* **2023**, *26*, e202200675.
[10] S. A. Cantalupo, S. R. Fiedler, M. P. Shores, A. L. Rheingold, L. H. Doerrer, *Angew. Chem. Int. Ed.* **2012**, *51*, 1000–1005.
[11] M. Cibian, S. Derossi, G. S. Hanan, *Dalton Trans.* **2011**, *40*, 1038–1040.
[12] Z. Mo, Y. Li, H. K. Lee, L. Deng, *Organometallics* **2011**, *30*, 4687–4694.
[13] A. Logallo, M. Mu, M. García-Melchor, E. Hevia, *Angew. Chem. Int. Ed.* **2022**, *61*, e202213246.
[14] M. Angeles García-Monforte, I. Ara, A. Martín, B. Menjón, M. Tomás, P. J. Alonso, A. B. Arauzo, J. I. Martínez, C. Rillo, *Inorg. Chem.* **2014**, *53*, 12384–12395.
[15] H.-B. Choi, J.-S. Ryu, W.-J. Shin, N. Vigier, *Nat. Commun.* **2019**, *10*, 5371.
[16] P. W. Gruber, P. A. Medina, G. A. Keoleian, S. E. Kesler, M. P. Everson, T. J. Wallington, *J. Ind. Ecol.* **2011**, *15*, 760–775.
[17] A. Logallo, E. Hevia, *Chem. Commun.* **2023**, *59*, 5383–5386.
[18] J. Contreras-García, E. R. Johnson, S. Keinan, R. Chaudret, J.-P. Piquemal, D. N. Beratan, W. Yang, *J. Chem. Theory Comput.* **2011**, *7*, 625–632.
[19] F. M. Bickelhaupt, *J. Comput. Chem.* **1999**, *20*, 114–128.
[20] E. D. Glendening, A. Streitwieser, *J. Chem. Phys.* **1994**, *100*, 2900–2909.
[21] E. D. Glendening, *J. Am. Chem. Soc.* **1996**, *118*, 2473–2482; G. K. Schenter, E. D. Glendening, *J. Phys. Chem.* **1996**, *100*, 17152–17156.
[22] M. Mantina, A. C. Chamberlin, R. Valero, C. J. Cramer, D. G. Truhlar, *J. Phys. Chem. A* **2009**, *113*, 5806–5812.

Manuscript received: June 19, 2023
Accepted manuscript online: July 26, 2023
Version of record online: September 12, 2023